Bragg reflection waveguides as integrated sources of entangled photon pairs

Sergei V. Zhukovsky,[1,*] Lukas G. Helt,[1] Payam Abolghasem,[2] Dongpeng Kang,[2] John E. Sipe,[1] and Amr S. Helmy[2]

[1]*Department of Physics and Institute for Optical Sciences, University of Toronto, 60 St. George Street, Toronto, Ontario M5S 1A7, Canada*

[2]*The Edward S. Rogers Department of Electrical and Computer Engineering, University of Toronto, 10 King's College Road, Toronto, Ontario M5S 3G4, Canada*

**Corresponding author: szhukov@physics.utoronto.ca*

Received January 5, 2012; accepted July 14, 2012;
posted July 23, 2012 (Doc. ID 160915); published August 28, 2012

We explore the potential of versatile and efficient entangled photon pair generation by spontaneous parametric downconversion in Bragg reflection waveguides. By employing a quantum treatment of modes in channel waveguides, and by accounting for group velocity dispersion in the modes, the quantum state of the generated biphotons is realistically calculated. The pair production rate is predicted to reach 4×10^8 pairs/s/nm/mW of pump light in a 2 mm-long structure, on par with or exceeding the performance of previously reported designs. This is attributable to an enhanced nonlinear interaction through tight mode confinement in the waveguide. Strategies for device performance optimization and phase matching wavelength tunability are outlined and numerically demonstrated. The proposed design platform is versatile and allows photon pair generation with controllable flux, bandwidth, Schmidt number, and degree of polarization entanglement. The possibility of monolithic integration with a diode laser pump offers a way to design an electrically pumped entangled photon source.

OCIS codes: 230.7380, 230.1480, 190.4975, 270.5565.

1. INTRODUCTION

Ongoing progress in quantum optical communication and information processing depends crucially on the availability of reliable, high-performance, versatile, and compact sources of entangled photon pairs. To this end, spontaneous parametric downconversion (SPDC) is widely employed because the generated photons are far away in frequency from both pump and Raman scattered photons, thus allowing operation at room temperature. However, conventional bulk-crystal SPDC suffers from low generation rates and collection efficiencies. To remedy this, waveguided SPDC sources are now in development, with improved performance due to tight lateral confinement of the waveguide modes [1]. Tightly confined waveguide modes are also more suitable for coupling into photonic circuits. Efficient photon pair generation has been achieved in periodically poled $LiNbO_3$ (PPLN), $KTiOPO_4$ (PPKTP), and $LiTaO_3$ (PPLT) waveguides [2–4].

A further improvement on this technology and its application to large-scale quantum information processing would be the ability to integrate photon pair sources with pump lasers and other optical components on a single chip. Although there has been considerable progress in the design of on-chip quantum interference circuitry [5–7], these designs still depend on an external entangled photon source, so bringing it onto the chip would be a timely advance for photonic quantum technologies. In this respect, $Al_xGa_{1-x}As$ is a particularly promising integration platform due to its large second-order nonlinearity, broad transparency window, good thermal conductivity, mature fabrication technology, and the possibility of monolithic integration with diode lasers, unlike $LiNbO_3$ or KTP.

Although $Al_xGa_{1-x}As$ lacks natural birefringence due to its zincblende crystal structure, exact phase matching (PM) in $\chi^{(2)}$-nonlinear processes can be achieved in Bragg reflection waveguides (BRWs) where downconverted (fundamental) modes are guided by total internal reflection and pump (second-harmonic) modes are guided by the Bragg mirrors in the cladding [8]. As these guiding mechanisms are largely independent, superior control over mode properties can be exerted, so that nonlinear mode coupling can be improved [9] and the dispersion of the modes can be manipulated [10]. Efficient frequency conversion processes, such as second-harmonic generation (SHG) [11], sum frequency generation [12], and difference frequency generation [13], have been demonstrated in recent experiments. A diode laser monolithically integrable into a BRW and capable of lasing into the Bragg-guided modes was also demonstrated [14], and using BRWs for SPDC with controlled bandwidth of the downconverted photons was proposed [10].

A conventional semiclassical description of downconversion processes [15] is faced with several limitations when applied to waveguides employing highly dispersive materials such as $Al_xGa_{1-x}As$, as the dispersion can significantly modify the quantum state of generated light across the operating bandwidth. Also, most semiclassical treatments can become inaccurate at pump intensities beyond low pair generation rates. To utilize the full potential of the compound semiconductor platform for entangled photon generation, an accurate quantum formalism is needed, which allows determination of

the state of generated photons realistically in high-efficiency processes and in the presence of both material and modal dispersion. Such a formalism for channel waveguides was developed recently [16] and applied to quasi-PM optical fibers [17].

In this paper, we theoretically study the entangled photon pair generation by SPDC in a BRW structure previously optimized for SHG [11]. The full Hamiltonian treatment we present, with an account of group velocity dispersion in the waveguide modes, is expected to result in a realistic prediction of generated entangled photon properties, especially in waveguides made of highly dispersive materials such as $Al_xGa_{1-x}As$ operating close to its band gap. Using numerically obtained pump and downconverted mode properties, we calculate the biphoton wave function (BWF) and indicate the limits on the applicability of this calculation due to waveguide losses. Within these limits, a quantitative prediction of the pair generation efficiency in BRWs can be made. It surpasses integrated topside-pumped $Al_xGa_{1-x}As$ structures [18–20] and is on par with or better than other waveguide devices [2,3]. Along with the generation rate, the Schmidt number (SN) for the generated biphotons is calculated, characterizing the entanglement in the biphoton states. A further improvement in efficiency is shown to be possible by varying the geometry and composition of the core. Finally, we quantitatively examine the tuning mechanisms and tuning ranges of the PM wavelength, λ_{PM}, through carrier injection and ambient temperature [21]. The results provide clues for optimizing entangled photon generation in new integrated designs.

The paper is organized as follows. Section 2 reviews the quantum Hamiltonian treatment of SPDC in channel waveguides. Section 3 follows with calculation results. The performance of the proposed entangled photon source and the properties of generated biphotons are discussed. In Sections 4 and 5, device optimization (via variation of structured-core parameters) and tunability (using thermal and carrier injection mechanisms) are further explored. Section 6 summarizes the paper.

2. SPDC IN BRAGG REFLECTION WAVEGUIDES

We consider a 2 mm-long structured-core BRW (Fig. 1) optimized for efficient SHG [11], reasonably expecting a high efficiency in the reverse process (i.e., SPDC) as well. In such a channel waveguide, SPDC can be described by the approach of Yang *et al.* [16] extended to account for polarization [17]. The nonlinear coupling Hamiltonian is

$$H_{\mathrm{NL}} = \sum_{\alpha\beta\gamma} \int \mathrm{d}k_1 \mathrm{d}k_2 \mathrm{d}k S_{\alpha\beta\gamma}(k_1,k_2,k) c^{\dagger}_{\alpha k_1} c^{\dagger}_{\beta k_2} b_{\gamma k} + \mathrm{H.c.}, \quad (1)$$

where the Greek subscripts denote polarization components (x,y,z) in the lab frame; $c_{\sigma k} \equiv a^{F}_{\sigma k}$ and $b_{\sigma k} \equiv a^{S}_{\sigma k}$ are boson mode operators for downconverted (F) and pump (S) photons, respectively, with wavenumber k and polarization σ. They obey the commutation relations $[a^{m}_{\sigma k}, a^{\dagger m'}_{\sigma' k'}] = \delta_{mm'}\delta_{\sigma\sigma'}\delta(k-k')$ for $m = F, S$.

A coherent state with an average number of SH photons $|\mu|^2$ is taken as an asymptotic input state, i.e., $|\psi_{\mathrm{in}}\rangle = \exp[\mu \int \mathrm{d}k \phi(k) b^{\dagger}_{\sigma k} - \mathrm{H.c.}]$. In the undepleted pump approximation, the asymptotic output state is then given by $|\psi_{\mathrm{out}}\rangle = \mathrm{e}^{\nu C^{\dagger}_{\mathrm{II}} - \mathrm{H.c.}} |\psi_{\mathrm{in}}\rangle$ [16,17] with

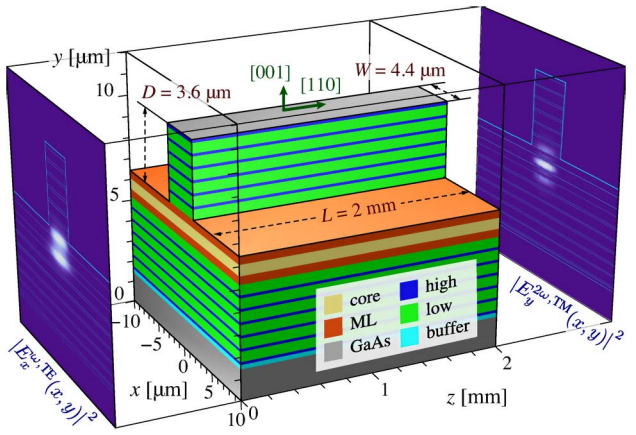

Fig. 1. (Color online) BRW ridge-waveguide structure under study. The core is a 500 nm $Al_{0.61}Ga_{0.39}As$ layer, surrounded by two 375 nm $Al_{0.2}Ga_{0.8}As$ matching layers (MLs). The Bragg mirrors are six-period quarter-wave stacks of 461 nm $Al_{0.7}Ga_{0.3}As$ and 129 nm $Al_{0.25}Ga_{0.75}As$. Also shown are intensity profiles of a TM-polarized pump mode (right) and a TE-polarized downconverted mode (left).

$$C^{\dagger}_{\mathrm{II}} = \frac{1}{\sqrt{2}} \sum_{\alpha,\beta} \int_0^{\infty} \mathrm{d}k_1 \mathrm{d}k_2 \phi_{\alpha\beta}(k_1,k_2) c^{\dagger}_{\alpha k_1} c^{\dagger}_{\beta k_2}. \quad (2)$$

Here, $\phi(k)$ defines the (normalized) pump pulse envelope function in k-space, and $\phi_{\alpha\beta}(k_1,k_2) = \phi_{\beta\alpha}(k_2,k_1)$ is the biphoton wave function (BWF) associated with a photon pair with wavenumbers k_1 and k_2 and polarizations α and β, respectively, with ν set so that [16,17]

$$\sum_{\alpha,\beta} \int |\phi_{\alpha\beta}(k_1,k_2)|^2 \mathrm{d}k_1 \mathrm{d}k_2 = 1. \quad (3)$$

Provided that the dispersion relations for the modes $k(\omega)$ are simple enough to allow one-to-one correspondence between wavenumber and frequency, we can redefine the ladder operators for the photons labeled by the frequency as $c_{\sigma\omega} \equiv c_{\sigma k(\omega)} \sqrt{dk^{\alpha}_{F}(\omega)/d\omega}$, introducing the BWF in frequency space as

$$\phi_{\alpha\beta}(\omega_1,\omega_2) = \sqrt{\frac{dk^{\alpha}_{F}(\omega_1)}{d\omega_1}} \sqrt{\frac{dk^{\beta}_{F}(\omega_2)}{d\omega_2}} \phi_{\alpha\beta}(k_1(\omega_1), k_2(\omega_2)) \quad (4)$$

to ensure proper normalization. With this in mind and appropriate approximations (see details in [16]), the expression for $|\nu|^2$ is

$$|\nu|^2 = |\mu|^2 \frac{(\bar{\chi}^{(2)})^2}{8\pi\varepsilon_0 \bar{n}^6} \frac{\hbar L^2}{v^{\alpha}_{F} v^{\beta}_{F} v^{\gamma}_{S} A_{\mathrm{eff}}} \times \int_0^{\infty} \mathrm{d}\omega_1 \mathrm{d}\omega_2 (\omega_1+\omega_2)\omega_1\omega_2 |\phi(\omega_1+\omega_2)\mathrm{sinc}(\Delta k^{\gamma\alpha\beta}_{\mathrm{PM}} L/2)|^2 \quad (5)$$

and in the limit $|\nu| \ll 1$, $|\nu|^2$ is the probability of pair generation per pump pulse. Here $\bar{\chi}_2$ and $\bar{n}$ are reference values of nonlinearity and refractive index (the actual values at different spatial points in the structure are accounted for when calculating the nonlinear interaction area A_{eff} [16]), and v^{σ}_{m} are the mode group velocities. One can show that if both the pump and the PM have a narrow bandwidth compared to the operating pump frequency, Eq. (5) coincides with the

semiclassical expression [15]. The quantity $|\nu|^2/|\mu|^2$ has the meaning of the expectation value for the number of generated pairs per pump photon for $|\nu| \ll 1$ and characterizes the efficiency of the entangled photon source.

The BWF in frequency space takes the well-known form [22,23]

$$\phi_{\alpha\beta}(\omega_1,\omega_2) \propto \phi(\omega_1+\omega_2)\mathrm{sinc}(\Delta k_{\mathrm{PM}}^{\gamma\alpha\beta}L/2), \tag{6}$$

where $\Delta k_{\mathrm{PM}}^{\gamma\alpha\beta} = k_S^{\gamma}(\omega_1+\omega_2) - k_F^{\alpha}(\omega_1) - k_F^{\beta}(\omega_2)$ is defined by the PM conditions. We consider both type-I and type-II PM, corresponding to copolarized and cross-polarized photons in a pair, respectively, and producing biphotons with polarization entanglement in the latter case. The mode dispersion relations around the PM frequency are taken as

$$k_{m=F,S}^{\sigma} = k_{m0}^{\sigma} + (\omega-\omega_{m0})/v_m^{\sigma} + (\omega-\omega_{m0})^2\Lambda_m^{\sigma}. \tag{7}$$

Here $\omega_{F0} = 2\pi c/\lambda_{\mathrm{PM}}$, where $\lambda_{\mathrm{PM}} = 1550$ nm is in the telecommunication range, and $\omega_{S0} = 2\omega_{F0}$ is the center pump frequency. Taking into account the group velocity dispersion in the normalization of the modes allows for a realistic treatment of structures made of materials operating close to their band gap and therefore having significant material dispersion, such as AlGaAs. The coefficients in Eq. (7) can be determined by fitting the function $k(\omega)$ obtained numerically from a full-vectorial commercial mode solver [24]. For type-I PM ($\gamma = y$, $\alpha = \beta = x$) in our structure $v_S^y = 74.3$ μm/ps, $v_F^x = 89.8$ μm/ps, $\Lambda_S^y = 2.92\times10^{-6}$ ps^2/μm, and $\Lambda_F^x = 7.07\times10^{-7}$ ps^2/μm. The type-II ($\gamma = \alpha = x$, $\beta = y$) values are within 1% of their type-I counterparts, except $\Lambda_S^x = 2.72\times10^{-6}$ ps^2/μm, which is less than Λ_S^y by around 4–5%.

The resulting BWFs in the form of probability density $|\phi_{\alpha\beta}(\omega_1,\omega_2)|^2$ for biphotons generated by type-I and type-II SPDC in the structure shown in Fig. 1 are plotted in Figs. 2(a) and 2(b).

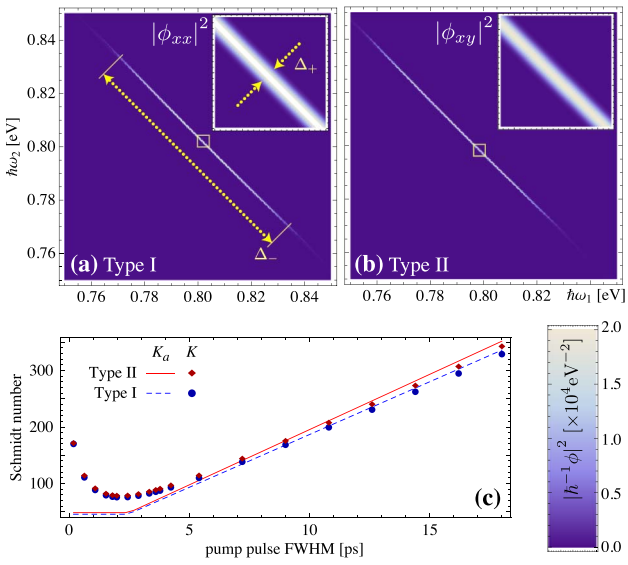

Fig. 2. (Color online) Density plots of the biphoton probability density $|\phi_{\alpha\beta}(\omega_1,\omega_2)/\hbar|^2$ in (a) type-I ($\alpha,\beta = x$) and (b) type-II ($\beta \neq \alpha$) PM. (c) The estimated (K_a) and numerically calculated (K) SN for the generated biphotons [see Eqs. (10) and (11)] depending on the pump pulse duration τ.

3. PROPERTIES OF GENERATED BIPHOTONS

We begin the analysis of the properties of generated photon pairs by calculating the generation efficiency, $|\nu|^2/|\mu|^2$, as given by Eq. (5). It is important to note [16] that if we had neglected the effects of group velocity dispersion in the normalization of the modes, we would have overestimated its value by about 28%.

For the more efficient type-II PM process, the efficiency is $|\nu|^2/|\mu|^2 = 2.54\times10^{-7}$, which is independent of the pump pulse duration if it is longer than about 1.5 ps. For 1.8 ps pump pulses with internal power of 0.01 mW and repetition rate of 76 MHz, this corresponds to about 0.13 photon pairs per pulse or 4.2×10^8 pairs/s/nm per mW of the pump. Taking into account the large bandwidth of downconverted signal (94 THz), the spectral brightness of the downconverted signal is 10.5 pairs/s/mW/MHz.

The type-I PM process is about three times less efficient because of a worse mode overlap for the TM-polarized pump [11]. The calculated efficiency is $|\nu|^2/|\mu|^2 = 0.78\times10^{-7}$ or 1.3×10^8 pairs/s/mW/nm (about 0.04 pairs/pulse) for the same pump pulses. It has a comparable but slightly narrower SPDC bandwidth (89 THz) and proportionally smaller spectral brightness (3.4 pairs/s/mW/MHz). We note that a large spectral bandwidth of downconverted photons can be beneficial if the proposed source is used in quantum optical coherence tomography [25,26].

In this theoretical description the waveguide is assumed to be completely lossless. In practice, both the pump and the downconverted modes are subject to losses, chiefly by two processes: one is the leakage of light out of the waveguide due to imperfect confinement (radiation losses), mainly in the Bragg modes. The other is the scattering of light due to surface roughness (scattering losses). Losses are more significant in Bragg modes (pump), where leakage losses can vary widely [between 5 and 50 dB/cm depending on many parameters including the Bragg stack confinement and the value of the etch depth D in a two-dimensional (2D) ridge]. Scattering losses, however, vary less than their leakage counterparts and are found to range between 2 and 10 dB/cm [27]. If the lower values of these ranges are to be used as a guide, the pump mode losses will only result in a reduction of the pair generation efficiency by 30–50% in a 2 mm-long waveguide. But excessive pump losses, in the range of 50–100 dB/cm, could modify the effective length of the sample, while maintaining a lower but nonzero rate of photon pair generation.

Losses in the downconverted, index-guided modes are more detrimental because the loss of one of the twin photons renders the pair unusable. Fortunately, with proper waveguide design, radiation losses in these modes are insignificant. Scattering losses can be made small as well. Recent results in upconversion experiments [11] show that they could be made below 8.5–9.5 dB/cm. By assuming that the expected probability of preserving both photons in a pair falls off with the propagation distance z as $P \sim \exp(-2\alpha z)$ where α is the loss coefficient, we find that a probability greater than e^{-1} of a pair being preserved holds for losses up to 10–11 dB/cm. Higher downconverted mode losses will require a more involved extension of the theory. Also noteworthy is that the imaginary parts in the propagation constants $k_{S,F}$ are not detrimental to PM for losses up to 10^3 dB/cm.

Owing to a high degree of confinement of optical modes in the waveguide and the enhanced nonlinear interaction between the modes due to the presence of MLs, the calculated pair production figures are very high for a broadband (i.e., non-cavity-enhanced) entangled photon source. In terms of efficiency, the proposed device is expected to surpass counterpropagating photon pair sources based on multilayer $Al_xGa_{1-x}As$ structures with unguided topside pumping [19,20] by 4 orders of magnitude. The proposed source also outperforms waveguide devices based on PPLN [2] and PPKTP [3], and is on par with recently introduced nanophotonic PPLN waveguides with tight confinement [28] where the generation rate of 4.8×10^{10} pairs/s/mW/nm was theoretically predicted in a 10 mm-long structure. At higher internal pumping powers of 10 mW (which is still realistic in experiments), the proposed device will generate $\sim10^{10}$ pairs/s, approaching the values predicted for electrically pumped quantum-well sources relying on a stronger process of stimulated two-photon emission [29,30].

It is instructive to compare the proposed BRWs with other $Al_xGa_{1-x}As$-based structures with guided pump modes (collinear propagation of pump and downconverted photons). One example is the previously reported structures with modal PM between lowest-order and higher-order modes guided by the same mechanism (total internal reflection) [31,32]. Simulated under the same condition as the proposed design, these structures offer even higher generation rates (by 3–4 times in type-I PM and by 5–7 times in type-II PM). However, the BRWs in our study have the advantage of offering exact PM between the *lowest-order* modes for both pump (propagating as a photonic band-gap mode) and downconverted photons (propagating due to total internal reflection). This facilitates the maximum mode interaction power available for the downconversion process. In contrast, a modal PM scheme employing higher-order index-guided modes can inherit higher propagation losses due to a slower exponential tail falloff than the fundamental Bragg-guided mode.

As seen from Eq. (6) and Fig. 2, the generated photons are strongly anticorrelated in frequency and the BWF is rather long and narrow in shape. The "width" Δ_+ (defined as the biphoton probability density FWHM along the line $\omega_1=\omega_2$) is influenced, on the one hand, by the bandwidth σ of the pump $\phi(\omega_1+\omega_2)=\exp[-(\omega_1+\omega_2-\omega_{S0})^2/\sigma^2]$, and on the other hand, by the group velocity mismatch (GVM) $\delta_v=|1/v_S-1/v_F|$. Thus $\Delta_+=\min(\sigma\sqrt{2\ln 2}, 4s/L\delta_v)$, where $s\approx1.39156$ is the root of $\mathrm{sinc}^2(s)=1/2$. The "length" Δ_- (i.e., the probability density FWHM along the line $\omega_1+\omega_2=2\omega_0$, which is also related to the SPDC bandwidth) is determined by the sample length and the group velocity dispersion of the downconverted mode. For the type-I PM, its value is

$$\Delta_-^{\mathrm{I}}=2\sqrt{4s/|\Lambda_F|L}. \tag{8}$$

For the type-II PM, there is a nonzero GVM between the TE- and TM-polarized downconverted biphotons ($\delta_v'=|1/v_F^x-1/v_F^y|\neq0$), slightly increasing the value of Δ_-:

$$\Delta_-^{\mathrm{II}}=2\sqrt{4s/|\Lambda_F|L+(\delta_v'/2|\Lambda_F|)^2}. \tag{9}$$

Note that this GVM was not present in previously studied entangled photon generation in periodically poled fiber [17], where the modes are degenerate with respect to polarization due to axial symmetry.

Such a marked anticorrelated character of generated biphotons essentially results from $v_S<v_F^x\approx v_F^y$, motivated by the focus of the present design on maximizing the strength of nonlinear mode interaction and pair generation efficiency. The versatility of the design platform, based on the independent waveguiding mechanisms for the pump and downconverted modes, allows more possibilities of controlling the BWF character. In general, the sinc function in Eq. (6) has its main lobe oriented in the (ω_1,ω_2)-plane at an angle given by $\tan^{-1}[(1/v_F^y-1/v_S)/(1/v_S-1/v_F^x)]$. If $2/v_S=1/v_F^x+1/v_F^y$, the sinc function would be perpendicular to the pump function in Eq. (6). Selection between correlated, uncorrelated, and anticorrelated photons could then be made by varying the pump bandwidth, similar to what was suggested earlier [33] for quasi-PM in BRWs.

The main challenge of achieving this property in the proposed design, which does not involve the costly process of structuring the core in the z-direction, is to have a sufficiently large $v_F^x-v_F^y$. This can be achieved by patterning the core on a subwavelength ($\sim$10 nm) scale, thus introducing artificial birefringence. We note that this subpatterning is compatible with $Al_xGa_{1-x}As$ fabrication processes because they allow the Al concentration x, and hence the refractive index, to vary on a much finer scale than the typical layer thickness in a Bragg mirror. The group velocity of Bragg-guided modes (v_S) can also be controlled by tailoring the Bragg cladding parameters, for example, by violating the quarter-wave condition commonly assumed in the claddings of BRWs.

The SPDC bandwidth could also be reduced by using the proposed structure in a cavity-enhanced configuration, such as by fabricating the waveguide in the form of a microring [34]. In addition to making the downconverted photons less strongly anticorrelated, which would be useful for heralding applications [35], the enhanced generation efficiency at ring resonances would further increase the spectral brightness of the proposed source there.

The degree of entanglement for the generated biphotons can be characterized by the Schmidt decomposition [36] $\phi_{\alpha\beta}(k_1,k_2)=\sum_n\sqrt{p_n}\chi_{n\alpha}(k_1)\chi_{n\beta}(k_2)$, where p_n are eigenvalues of the matrix $\rho_{k'k}^{\alpha\beta}=\int\phi_{\alpha\beta}^*(k',k'')\phi_{\alpha\beta}(k,k'')\mathrm{d}k''$, with $\sum_n p_n=1$. The quantity

$$K=\left[\sum\nolimits_n p_n^2\right]^{-1} \tag{10}$$

is called the Schmidt number (SN) [36]. It is greater than unity in the presence of entanglement. It is rather common to approximate the real BWF with a 2D Gaussian with FWHMs $\Sigma_\pm$ [18,23], in which case the SN is given by

$$K_a=(\Sigma_+^2+\Sigma_-^2)/2\Sigma_+\Sigma_-. \tag{11}$$

The FWHMs of the BWF $\Sigma_\pm$ are closely related to the corresponding FWHMs of the biphoton probability density $\Delta_\pm$ as $\Sigma_+=\Delta_+\sqrt{2}$ and $\Sigma_-=\Delta_-\sqrt{s'/s}\approx1.167\Delta_-$, where s' is the root of $\mathrm{sinc}(s)=1/2$. Figure 2(c) shows the dependence of the estimated versus numerically calculated SN on the pump pulse duration τ. For $\tau>3$ ps, both K and K_a depend linearly on τ with good coincidence. The slope of K_a slightly exceeds

that of K because $\mathrm{sinc}(\omega^2 \Lambda L/2)$ has a flatter variation than a Gaussian with the same FWHM. For $\tau < 1.5$ ps, σ becomes so large that the BWF includes sidelobes of the sinc function in Eq. (6). The effective value of Δ_- becomes larger than what Eq. (9) predicts, so K deviates from K_a and increases again. Between the two trends, where $\sigma\sqrt{2\ln 2} \simeq 4s/L\delta_v$, i.e., for $\tau \simeq 2$ ps, there is a minimum in the SN. At the minimum, $K \simeq 75$. A particularly promising regime would be the generation of completely separable photons, which involves reducing K towards unity. From the previous results, it is expected that both reducing the BRW ridge width W [10] and using BRW-based microrings [35] should be capable of achieving this regime.

Turning to specific applications, we examine how well the generated biphotons are suited for time-bin entanglement in type-I PM and for polarization entanglement in type-II PM. In the former, the goal is to create one pair per pump pulse as often as possible, while at the same time avoid creating more complicated output (such as four-photon states). The relevant figure of merit would be the "cost" of such generation in the form of the energy of a pump pulse required to achieve a predefined $|\nu|^2 < 1$. For the structure under study, this energy equals 4 pJ times the target value of $|\nu|^2$, i.e., 0.4 pJ for $|\nu|^2 = 0.1$.

Polarization entanglement is more complex. Asymmetry between TE- and TM-polarized downconverted photons causes each component of the BWF ϕ_{xy} to be asymmetric with respect to λ_{PM} [Fig. 2(b)]. While the condition $\phi_{xy}(\omega_1, \omega_2) = \phi_{yx}(\omega_2, \omega_1)$ always holds, the condition

$$\phi_{xy}(\omega_1, \omega_2) = \phi_{yx}(\omega_1, \omega_2) \tag{12}$$

is satisfied only approximately [see Fig. 2(b)]. Hence the state of generated biphotons will deviate from a polarization entangled state in which no information about a photon polarization can be inferred from its spectral properties. A corresponding figure of merit can be introduced as [37]

$$G = 2\int_0^\infty \mathrm{d}\omega_1 \mathrm{d}\omega_2 \phi_{xy}(\omega_1, \omega_2)\phi_{xy}^*(\omega_2, \omega_1), \tag{13}$$

where the factor of 2 results from the chosen normalization condition (3). If Eq. (12) holds, G attains its maximum value of 1. The resulting value for the structure under study is $G = 0.65$, which means that mild spectral postfiltering is required to use the proposed source for cryptographic purposes. Increasing the pump pulse duration would also increase G (see [22]), as would any method of reducing the GVM parameter δ_v'. The latter can be achieved by choosing an appropriate relation between the ridge width W, the total core thickness for the downconverted modes [38,39], and the cladding parameters. The possibility of introducing form birefringence in the selected layers by subwavelength index modulation provides an additional degree of freedom.

4. PARAMETER OPTIMIZATION

So far we have focused on the structure presented in Fig. 1, which was optimized for efficient SHG [11]. The design of this structure was obtained as a result of optimization of structured-core parameters, in particular, the Al concentration and thickness of the core and MLs [9]. It was shown that these parameters affect both the nonlinear efficiency and the mode dispersion properties, and hence can be used as additional degrees of freedom to optimize or control the properties of SPDC.

Here we analyze the dependence of several properties of biphoton generation on Al concentration in the core (x_c) and MLs (x_m). The core thickness t_c is kept constant at 500 nm. The ML thickness t_m is chosen so that the Bragg mirrors remain quarter-wave for the pump mode [9].

The SPDC bandwidth uniformly broadens for smaller x_c and larger x_m from 85 THz at $x_c = 0.66$, $x_m = 0.18$ to 95 THz at $x_c = 0.55$, $x_m = 0.25$ for type-I PM. For type-II PM there is a similar change from 90 to 99 THz. This result is associated with the dependence of Δ_- on the group velocity dispersion Λ_F [see Eqs. (8) and (9)], which in turn depends on x_c and x_m. These dependencies are consistent with previous results on SHG in slab BRWs [9].

The biphoton generation efficiency undergoes a rather uniform increase as x_m decreases (in practice limited by absorption losses below $x_m = 0.18$), as seen in Fig. 3. This is associated with bringing the operating point of the device closer to the band gap in $\mathrm{Al}_x\mathrm{Ga}_{1-x}\mathrm{As}$, which increases its effective nonlinearity. The dependence on x_c is generally nonmonotonic with optimal values of x_c in the range of

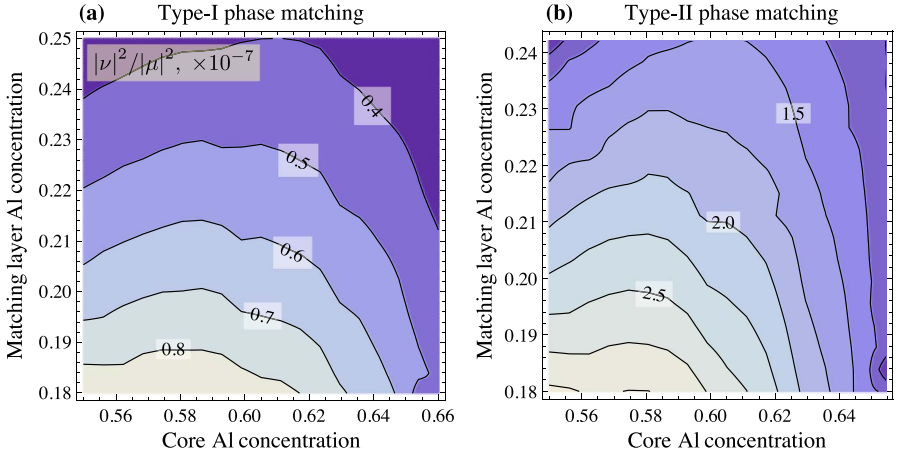

Fig. 3. (Color online) Dependence of biphoton generation efficiency $|\nu|^2/|\mu|^2$ on the properties of the structured core for type-I and type-II PM. The jagged features in the contours are artifacts of mesh discretization in the 2D mode solver.

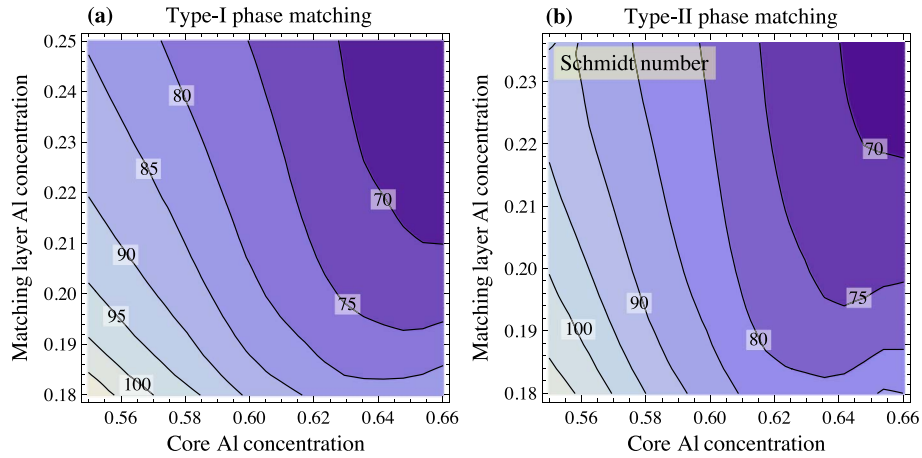

Fig. 4. (Color online) Dependence of the SN, K, on the properties of the structured core for type-I and type-II PM.

0.58 to 0.6. Throughout the parameter range, type-II SPDC remains about three times more efficient than type-I. The dependence for spectral brightness follows that for the efficiency, given that the variation in the generation bandwidth is uniform and relatively minor.

The increase in the biphoton generation rate is accompanied by a moderate increase of the SN by about 30–40% (Fig. 4). Changing the ridge width, on the other hand, was shown to alter the bandwidth of generated biphotons, and hence the SN, very significantly [10]. In agreement with Fig. 2(c), the type-II SN is slightly higher than the type-I.

The energy cost of producing a pair per pump pulse with probability 10% (the time-bin entanglement figure of merit) was found to vary between 0.3 and 0.8 pJ of internal pulse energy with the dependence very similar to that depicted in Fig. 3(a). The optimal parameters are achieved at $x_c \simeq 0.59$ and $x_m < 0.2$. Finally, the factor G given by Eq. (13) was found to range between 0.6 near the optimum generation region to 0.75 away from it. In the class of structures studied here, photons from a brighter source need more spectral filtering to be utilized in practical quantum cryptography schemes relying on polarization entanglement.

5. TUNING MECHANISMS

The $Al_xGa_{1-x}As$ fabrication platform can be subject to both thermally and electrically induced tuning [21]. Changing the ambient temperature causes a shift in the refractive indices of all the layers in the structure, accounted for by the Gehrsitz model [40]. Figure 5(a) shows the resulting linear shift in λ_{PM} of about 0.11–0.12 nm/K in both type-I and type-II PM. Figure 6(a) indicates that the pair production rate increases with temperature, but very slightly. This makes thermal tuning a suitable compensation mechanism to counteract an operational wavelength shift due to fabrication imperfections or changes in the environment.

For carrier injection tuning, which relies on the dependence of the refractive index of AlGaAs on free carrier concentration, the structure could be doped with a p-i-n profile. The intrinsic region (in our case, the core and MLs) becomes the volume where carriers are injected if the resulting p-i-n transition is forward biased [21]. We assume the refractive index to shift by $\Delta n = (-1.2 \times 10^{-20}\ \mathrm{cm}^3)N$, where N is the carrier concentration ranging from $10^{18}\ \mathrm{cm}^{-3}$ up to $10^{19}\ \mathrm{cm}^{-3}$. In this case [Fig. 5(b)], λ_{PM} changes more noticeably and depends on N in a nonlinear fashion, shifting by 30 nm for $N = 4 \times 10^{18}\ \mathrm{cm}^{-3}$. It is seen that the pair production rate tends to decrease for greater carrier densities [Fig. 6(b)] but the changes become significant only for $N > 3 \times 10^{18}\ \mathrm{cm}^{-3}$. Note that type-I and type-II tuning curves cross just below $N = 3 \times 10^{18}\ \mathrm{cm}^{-3}$. Thus, carrier injection can exert control not only over λ_{PM} itself but also over how the two different channels of SPDC are manifest in the same structure. This can be used in applications involving multiple-channel SPDC [41].

We recall that downconverted mode losses need to remain below 10–11 dB/cm for the presented results to be valid; see the discussion in Section 3. This may no longer hold for some device configurations. For example, if carrier injection is used for tuning the PM condition, free carrier absorption will take place and eventually limit the tuning range. As determined from recent measurements for BRW lasers, which also use doped AlGaAs layers, overall mode losses there can rise to be in the range of 20–25 dB/cm [14,42].

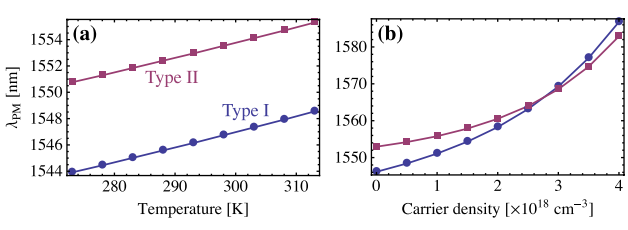

Fig. 5. (Color online) Dependence of PM wavelength on (a) ambient temperature and (b) injection of carriers into the core and MLs.

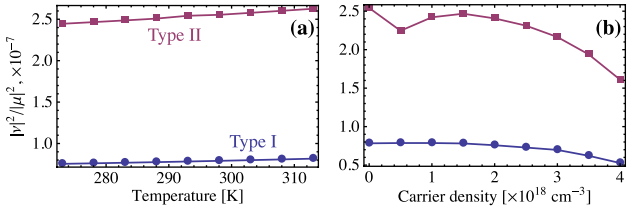

Fig. 6. (Color online) Dependence of pair production rate on (a) ambient temperature and (b) injection of carriers into the core and MLs. The lines are a guide to the eye.

6. CONCLUSION

In conclusion, we have applied a quantum description of SPDC to BRWs. We have demonstrated that BRWs can act as versatile and high-performance sources of entangled photon pairs in the telecommunication wavelength range. The source can be monolithically integrated with a laser diode pump, as well as with other components on an $Al_xGa_{1-x}As$ optical chip. The predicted generation rate in a 2 mm-long structure is up to 4×10^8 pairs/s/mW/nm, or a few pairs per pump pulse with internal energy as low as 1.5 pJ. The device is based on existing state-of-the-art fabrication techniques [11] and is experimentally realizable. A very recent paper [43] has indeed reported an experiment showing photon pair generation in a BRW.

ACKNOWLEDGMENTS

The authors would like to thank Y. Soudagar, X. Xing, and M. Liscidini for helpful comments. This work was supported by the Natural Sciences and Engineering Research Council of Canada (NSERC).

REFERENCES

1. M. Fiorentino, S. M. Spillane, R. G. Beausoleil, T. D. Roberts, P. Battle, and M. W. Munro, "Spontaneous parametric down-conversion in periodically poled KTP waveguides and bulk crystals," Opt. Express **15**, 7479–7488 (2007).
2. G. Fujii, N. Namkata, M. Motoya, S. Kurimura, and S. Inoue, "Bright narrowband source of photon pairs at optical telecommunication wavelengths using a type-II periodically poled lithium niobate waveguide," Opt. Express **15**, 12769–12776 (2007).
3. J. Chen, A. J. Pearlman, A. Ling, J. Fan, and A. Migdall, "A versatile waveguide source of photon pairs for chip-scale quantum information processing," Opt. Express **17**, 6727–6740 (2009).
4. M. Lobino, G. D. Marshall, C. Xiong, A. S. Clark, D. Bonneau, C. M. Natarajan, M. G. Tanner, R. H. Hadfield, S. N. Dorenbos, T. Zijlstra, V. Zwiller, M. Marangoni, R. Ramponi, M. G. Thompson, B. J. Eggleton, and J. L. O'Brien, "Correlated photon-pair generation in a periodically poled MgO doped stoichiometric lithium tantalate reverse proton exchanged waveguide," Appl. Phys. Lett. **99**, 081110 (2011).
5. J. L. O'Brien, A. Furusawa, and J. Vučković, "Photonic quantum technologies," Nat. Photon. **3**, 687–695 (2009).
6. M. G. Thompson, A. Politi, J. C. F. Matthews, and J. L. O'Brien, "Integrated waveguide circuits for optical quantum computing," IET Circuits, Devices Syst. **5**, 94–102 (2011).
7. L. Sansoni, F. Sciarrino, G. Vallone, P. Mataloni, A. Crespi, R. Ramponi, and R. Osellame, "Polarization entangled state measurement on a chip," Phys. Rev. Lett. **105**, 200503 (2010).
8. A. S. Helmy, "Phase matching using Bragg reflection waveguides for monolithic nonlinear optics applications," Opt. Express **14**, 1243–1252 (2006).
9. P. Abolghasem and A. S. Helmy, "Matching layers in Bragg reflection waveguides for enhanced nonlinear interaction," IEEE J. Quantum Electron. **45**, 646–653 (2009).
10. P. Abolghasem, M. Hendrych, X. Shi, J. P. Torres, and A. S. Helmy, "Bandwidth control of paired photons generated in monolithic Bragg reflection waveguides," Opt. Lett. **34**, 2000–2002 (2009).
11. P. Abolghasem, J. Han, B. J. Bijlani, A. Arjmand, and A. S. Helmy, "Highly efficient second-harmonic generation in monolithic matching layer enhanced $Al_xGa_{1-x}As$ Bragg reflection waveguides," IEEE Photon. Technol. Lett. **21**, 1462–1464 (2009).
12. J. Han, P. Abolghasem, B. J. Bijlani, and A. S. Helmy, "Continuous-wave sum-frequency generation in AlGaAs Bragg reflection waveguides," Opt. Lett. **34**, 3656–3658 (2009).
13. J. Han, P. Abolghasem, D. Kang, B. J. Bijlani, and A. S. Helmy, "Difference-frequency generation in AlGaAs Bragg reflection waveguides," Opt. Lett. **35**, 2334–2336 (2010).
14. B. J. Bijlani and A. S. Helmy, "Bragg reflection waveguide diode lasers," Opt. Lett. **34**, 3734–3736 (2009).
15. A. De Rossi, V. Berger, M. Calligaro, G. Leo, V. Ortiz, and X. Marcadet, "Parametric fluorescence in oxidized aluminum gallium arsenide waveguides," Appl. Phys. Lett. **79**, 3758–3760 (2001).
16. Z. Yang, M. Liscidini, and J. E. Sipe, "Spontaneous parametric down-conversion in waveguides: a backward Heisenberg picture approach," Phys. Rev. A **77**, 033808 (2008).
17. L. G. Helt, E. Y. Zhu, M. Liscidini, Li Qian, and J. E. Sipe, "Proposal for in-fiber generation of telecom-band polarization-entangled photon pairs using a periodically poled fiber," Opt. Lett. **34**, 2138–2140 (2009).
18. X. Caillet, V. Berger, G. Leo, and S. Ducci, "A semiconductor source of counterpropagating twin photons: a versatile device allowing the control of the two-photon state," J. Mod. Opt. **56**, 232–239 (2009).
19. X. Caillet, A. Orieux, A. Lemaître, P. Filloux, I. Favero, G. Leo, and S. Ducci, "Two-photon interference with a semiconductor integrated source at room temperature," Opt. Express **18**, 9967–9975 (2010).
20. A. Orieux, X. Caillet, A. Lemaître, P. Filloux, I. Favero, G. Leo, and S. Ducci, "Efficient parametric generation of counterpropagating two-photon states," J. Opt. Soc. Am. B **28**, 45–51 (2011).
21. B. R. West and A. S. Helmy, "Analysis and design equations for phase matching using Bragg reflector waveguides," IEEE J. Sel. Top. Quantum Electron. **12**, 431–442 (2006).
22. W. P. Grice and I. A. Walmsley, "Spectral information and distinguishability in type-II down-conversion with a broadband pump," Phys. Rev. A **56**, 1627–1634 (1997).
23. W. P. Grice, A. B. U'Ren, and I. A. Walmsley, "Eliminating frequency and space-time correlations in multiphoton states," Phys. Rev. A **64**, 063815 (2001).
24. Mode Solutions, version 4.0, Lumerical Solutions, Inc. Available: http://www.lumerical.com.
25. A. F. Abouraddy, M. B. Nasr, B. E. A. Saleh, A. V. Sergienko, and M. C. Teich, "Quantum-optical coherence tomography with dispersion cancellation," Phys. Rev. A **65**, 053817 (2002).
26. M. B. Nasr, B. E. A. Saleh, A. V. Sergienko, and M. C. Teich, "Dispersion-cancelled and dispersion-sensitive quantum optical coherence tomography," Opt. Express **12**, 1353–1362 (2004).
27. C. Tong, B. J. Bijlani, L. S. Zhao, S. Alali, Q. Han, and A. S. Helmy, "Mode selectivity in Bragg reflection waveguide lasers," IEEE Photon. Technol. Lett. **23**, 1025–1027 (2011).
28. S. M. Spillane, M. Fiorentino, and R. G. Beausoleil, "Spontaneous parametric down conversion in a nanophotonic waveguide," Opt. Express **15**, 8770–8780 (2007).
29. A. Hayat, P. Ginzburg, and M. Orenstein, "High-rate entanglement source via two-photon emission from semiconductor quantum wells," Phys. Rev. B **76**, 035339 (2007).
30. A. Hayat, P. Ginzburg, and M. Orenstein, "Observation of two-photon emission from semiconductors," Nat. Photon. **2**, 238–241 (2008).
31. S. Ducci, L. Lanco, V. Berger, A. De Rossi, V. Ortiz, and M. Calligaro, "Continuous-wave second-harmonic generation in modal phase matched semiconductor waveguides," Appl. Phys. Lett. **84**, 2974–2976 (2004).
32. A. De Rossi, V. Ortiz, M. Calligaro, B. Vinter, J. Nagle, S. Ducci, and V. Berger, "A third-order-mode laser diode for quantum communication," Semicond. Sci. Technol. **19**, L99–L102 (2004).
33. J. Svozilík, M. Hendrych, A. S. Helmy, and J. P. Torres, "Generation of paired photons in a quantum separable state in Bragg reflection waveguides," Opt. Express **19**, 3115–3123 (2011).
34. Z. Yang, P. Chak, A. D. Bristow, H. M. van Driel, R. Iyer, J. S. Aitchison, A. L. Smirl, and J. E. Sipe, "Enhanced second-harmonic generation in AlGaAs microring resonators," Opt. Lett. **32**, 826–828 (2007).
35. L. G. Helt, Z. S. Yang, M. Liscidini, and J. E. Sipe, "Spontaneous four-wave mixing in microring resonators," Opt. Lett. **35**, 3006–3008 (2010).
36. C. K. Law and J. H. Eberly, "Analysis and interpretation of high transverse entanglement in optical parametric down conversion," Phys. Rev. Lett. **92**, 127903 (2004).

37. T. S. Humble and W. P. Grice, "Effects of spectral entanglement in polarization-entanglement swapping and type-I fusion gates," Phys. Rev. A **77**, 022312 (2008).
38. K. Seng Chiang and W. Peng Wong, "Theory of zero-birefringence multiple-quantum-well optical waveguides," IEEE J. Quantum Electron. **35**, 1554–1564 (1999).
39. W. Peng Wong and K. Seng Chiang, "Design of polarization-insensitive Bragg gratings in zero-birefringence ridge waveguides," IEEE J. Quantum Electron. **37**, 1138–1145 (2001).
40. S. Gehrsitz, F. K. Reinhart, C. Gourgon, N. Herres, A. Vonlanthen, and H. Sigg, "The refractive index of $Al_xGa_{1-x}As$ below the band gap: accurate determination and empirical modeling," J. Appl. Phys. **87**, 7825–7837 (2000).
41. S. Gao and C. Yang, "Two channels of entangled twin photons generated by quasi-phase-matched spontaneous parametric down-conversion in periodically poled lithium niobate crystals," J. Opt. Soc. Am. B **25**, 734–740 (2008).
42. C. Tong, B. J. Bijlani, S. Alali, and A. S. Helmy, "Characteristics of edge-emitting Bragg reflection waveguide lasers," IEEE J. Quantum Electron. **46**, 1605–1610 (2010).
43. R. Horn, P. Abolghasem, B. J. Bijlani, D. Kang, A. S. Helmy, and G. Weihs, "Monolithic source of photon pairs," Phys. Rev. Lett. **108**, 153605 (2012).